Ain Shams Engineering Journal xxx (xxxx) xxx

Contents lists available at ScienceDirect

Ain Shams Engineering Journal

journal homepage: www.sciencedirect.com

Electrical Engineering

# Study of a current multilevel converter as an interconnection element for PV systems

R. Hernandez [a,*], V. Cardenas [a], G. Espinoza-Perez [b], R. Alvarez-Salas [a], H. Miranda-Vidales [a]

[a] *Autonomous University of San Luis Potosí, San Luis Potosí, Mexico*
[b] *National Autonomous University of Mexico, Cd. de México, Mexico*

ARTICLE INFO

*Article history:*
Received 2 January 2021
Revised 15 April 2021
Accepted 26 June 2021
Available online xxxx

*Keywords:*
Current source converter
Multilevel current rectifier
PV system

ABSTRACT

The present paper focuses on the use of the Multilevel Current Rectifier topology as an interconnection element between PV systems and the network or loads. In order to properly use the converter in connection with the PV system, several subjects such as the compatibility with the maximum power point tracking and the compatibility between the converter and the PV array must be taken into account. Compatibility between the converter and the PV array can be achieved by ensuring at least the maximum power point is a point that the converter can work with. In this sense, this work focuses on the operating conditions to guarantee the compatibility with the PV array. The main results are an analytical and experimental characterization of the operating range of the system using the Multilevel Current Rectifier. This operating range has a precision of 1%. Leading to the conclution that not only the converter is a viable option, but also that the theory and methodology used can be extrapolated to another topologies.



## 1. Introduction

The incorporation of renewable energy sources for electrical power generation raises the need for power electronic converters. Photovoltaic (PV) systems require viable converter topologies [1–3], which, in addition to being functional, need to improve system reliability. Modular topologies of power electronic converters have shown favorable characteristics to improve such reliability. A suitable topology is the Multilevel Current Rectifier (MCR) [4] which has the properties of natural control of the current, higher reliability due to being a modular converter, reduced harmonic distortion in the output current (because it is a multilevel topology). In contrast with the Voltage Source Converter (VSC) solutions, these properties can improve PV system performance. This added to the fact that the PV arrays are modeled as a current source that depends on the voltage, temperature and solar radiance [5–7] make a Current Source Converter (CSC) a convenient option for the interconnection of PV systems.

The problem addressed in this work is the study of the MCR as a viable topology for interconnecting a PV system, showing its correct operation not only experimentally but also analytically. These results are obtained under conditions that ensure the correct operation, as well as the characterization of the operable regions and their restrictions.

The problem of the correct operation when the power converter and the PV system work together has been reported in [8–14] which are works focused on DC-DC topologies. Those works see the converter as a variable resistance depending on the modulation and the duty cycle. This approach only works with an operation point at the time and it does not work with a set of infinite operation points.

The study of CSC as an interconnection element for PV systems is reported in [15,16], and the use of multilevel current source topologies such as the MCR is reported in [17,18]. The previous contributions focus on the study and simulation of the system that achieves the control of the current delivered to the electrical grid, but leaving aside the application (like the interconnection of renewable energy sources or the operation as an active filter, among others). In addition, the reported works studying the MCR use reduced models of the systems.

The methodology used in this paper is based on the use of the dynamic equations of the converter and its equilibrium point. Then, expressions that relate the signals form the panel $(V_{pv}, I_{pv})$ with the output of the converter can be obtained. Next, the Inverse function and Implicit function theorems are used to show that for every input point $(V_{pv}, I_{pv})$ exists an output point given by the converter. Finally, the operation of the system converter-PV is checked

* Corresponding author at: Autonomous University of San Luis Potosi, Engineering Faculty, Dr. Manuel Nava # 8, Zona Universitaria Poniente C.P. 78290, San Luis Potosí, S.L.P, Mexico

*E-mail address:* rafael.jesus.hh@gmail.com (R. Hernandez).

https://doi.org/10.1016/j.asej.2021.06.027
2090-4479/

via an experimental prototype. A summarized version of the methodology is presented in Fig. 1.

The contribution of the work can be summarized in two main points: first, to achieve the interconnection of a PV system via the MCR topology; second, to guarantee analytically and experimentally that the MCR-PV system works correctly. The work is structured as follows: Section II shows the topology of the MCR together with the model; Section III presents the model in the DQ frame in order to work with equilibrium points, and through these equations the maximum achievable working point for the converter is established. Section IV the equilibrium equations are rearranged as coordinate functions, and using the Jacobian it is proved that each point in the PV array has a working point along with the converter. Section V several simulations are presented in order to show the effects of not fulfilling the conditions obtained in previous sections. Section VI presents the experimental results of the converter working as an interconnection element for a PV array to show the correct operation; in Section VII the discussion of the results is included. Finally, in the Conclusions section, the main results and their limitations are highlighted establishing possible future work.

## 2. Converter description and model

The MCR considered in this paper is shown in Fig. 2. The parallel connection of cells gives the converter the modular structure and allows multilevel output current as a result of the division of the $i_{dc}$ evenly among the cells. The $i_{pwm}$ output current is a function of the modulation signals and the currents $i_{Lh1}, i_{Lh2}, \ldots, i_{lhn}, i_{Ll1}, i_{Ll2}, \ldots, i_{Lln}$ in the cells. The system is described using the average state Eqs. (1)–(6) using the notation for the signals $i_{Lh1} = x_1, i_{Lh2} = x_2, i_{Ll1} = y_1, i_{Ll2} = y_2, i_L = x_6, v_c = x_5$ for the case where the MCR has $n = 2$ cells.

$$L_{h1}\dot{x}_1 = -[(u_1 - \bar{u}_1) - (u_2 - \bar{u}_2)]\frac{x_5}{2n} - x_1R_1 \tag{1}$$

$$L_{h2}\dot{x}_2 = -[(u_2 - \bar{u}_2) - (u_1 - \bar{u}_1)]\frac{x_5}{2n} - x_2R_2 \tag{2}$$

$$L_{l1}\dot{y}_1 = -[(v_1 - \bar{v}_1) - (v_2 - \bar{v}_2)]\frac{x_5}{2n} - y_1R_1 \tag{3}$$

$$L_{l2}\dot{y}_2 = -[(v_2 - \bar{v}_2) - (v_1 - \bar{v}_1)]\frac{x_5}{2n} - y_2R_2 \tag{4}$$

$$C\frac{dx_5}{dt} = i_{pwm} - x_6 \tag{5}$$

$$L\frac{dx_6}{dt} = x_5 - v_r \tag{6}$$

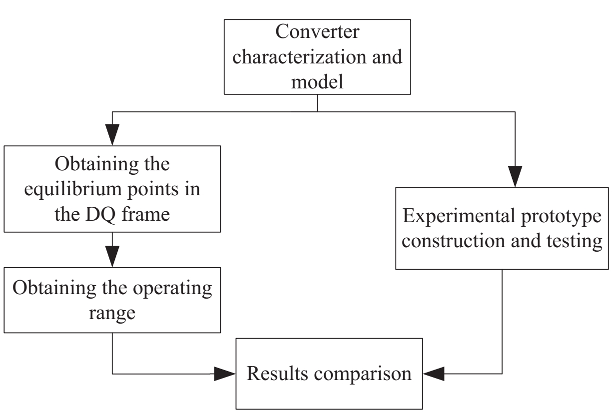


**Fig. 1.** Methodology used in the research.

Eqs. (1)–(4) describe the dynamic behavior of the current in the cells; Eqs. (5) and (6) describe the dynamic behavior of the rest of the system. All equations are obtained using Kirchhoff's laws. Terms $u_k$ and $v_k$ are the upper and lower modulation signals of the $k$-th switch, and $\bar{u}_k, \bar{v}_k$ their corresponding logical complement. The grid voltage is defined as $v_r = v_r^d sin(wt)$. The current $i_{pwm}$ goes through the second order filter and it is defined in the Eqn (7).

$$\begin{aligned} i_{pwm} &= \tfrac{1}{2}[x_1(u_1 - \bar{u}_1) + x_2(u_2 - \bar{u}_2) \\ &\quad -y_1(v_1 - \bar{v}_1) - y_2(v_2 - \bar{v}_2)] \end{aligned} \tag{7}$$

The model is developed using considerations like reducing the redundant commutation states and reduced unbalance conditions. The differences in the commutations signals (related to the modulations signals $u_k, v_k$), or the differences between the losses in the cells, generate unbalanced operation conditions which is reflected in uneven energy and currents $i_{Lhk/l}$ in the cells. Also the unbalance conditions affect the multilevel output current not allowing the correct harmonic cancellation.

## 3. MCR compatibility with the PV array

The approach to ensure the compatibility between the converter and the PV array is taking the equations of the model (1)–(6), and noticing that even with unbalance conditions the model equations can be described via an output current, without using explicitly the modules currents $i_{Lhk}/i_{Llk}$. The interaction among the converter, the PV array and the grid can be described using the Eqs. (5), (6) applying the single-phase DQ transformation to describe the steady state of the converter as an equilibrium point in the DQ frame, resulting in the expressions (8), (9). The $d$ term is the direct component and the $q$ term is the quadrature component, while $w$ is the grid frequency (see Table 1).

$$\mathbf{0} = \begin{bmatrix} 0 & Cw & -1 & 0 \\ -Cw & 0 & 0 & -1 \\ 1 & 0 & 0 & Lw \\ 0 & 1 & -Lw & 0 \end{bmatrix} \mathbf{x}^{dq} - \begin{bmatrix} 0 & 0 & 0 & 0 \\ 0 & 0 & 0 & 0 \\ 0 & 0 & R & 0 \\ 0 & 0 & 0 & R \end{bmatrix} \mathbf{x}^{dq} + \begin{bmatrix} u^d & u^q & 0 & 0 \end{bmatrix}^T i_{dc} \tag{8}$$

$$\mathbf{x}^{dq} = \begin{bmatrix} x_5^d & x_5^q & x_6^d & x_6^q \end{bmatrix}^T \tag{9}$$

In the equations above $u^d$ and $u^q$ are the resulting signals form the DQ map over the modulation signal $u$. These equilibrium equations are complemented by adding the $v_{dc}$ voltage equation given by:

$$v_{dc} = [u_1 - \bar{u}_1 + u_2 - \bar{u}_2 + v_1 - \bar{v}_1 + v_2 - \bar{v}_2]\frac{x_5}{4} = ux_5 \tag{10}$$

which is equivalent to (11) in the DQ frame.

$$v_{dc} = \frac{1}{2}(u^d v_c^d + u^q v_c^q) \tag{11}$$

In order to achieve the Maximum Power Point (MPP) of the PV array with the converter, an additional condition must be added: the maximum value for the modulation signal $u$ must be less or equal to 1, $\|u^{dq}\| \leqslant 1$. Working with the Eq. (9) results in the expressions:

$$u^d = \frac{i_L^d(1 - CLw^2)}{i_{dc}} \tag{12}$$

$$u^d = \frac{CwV_r^d}{i_{dc}} \tag{13}$$

Substituting the previous equations on the Eq. (11) results in the expression (14):

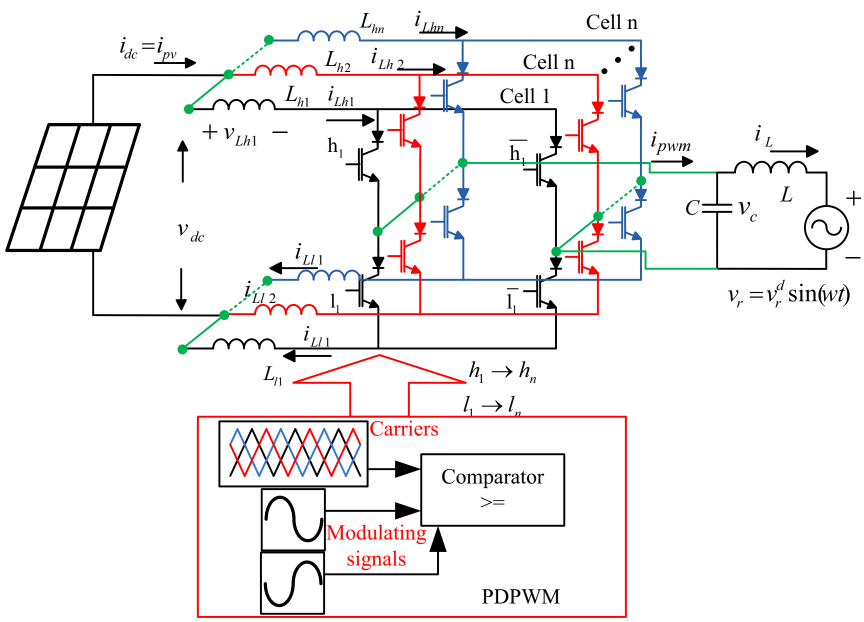


**Fig. 2.** Multilevel Current Rectifier (MCR).

**Table 1**
Nomenclature.

| | |
|---|---|
| $i_{pv}/i_{dc}$ | DC current bus/PV current |
| $i_{Lh}/x_k$ | Current on the upper inductor of the cells |
| $i_{Llk}/y_k$ | Current on the lower inductors of the cells |
| $i_{pwm}$ | Multilevel pulsating current |
| $i_L/x_6$ | Output current to the grid |
| $v_{dc}/v_{pv}$ | DC voltage/ PV voltage |
| $v_c/x_5$ | Capacitor voltage of the second order filter |
| $v_r$ | Voltage of the grid |
| $v_r^d$ | Peak value of the grid voltage |
| $v_{Lhk/lk}$ | Voltage of the inductor of the cells |
| $h_k/\bar{h}_k/l_k/\bar{l}_k$ | Switches of the cells |
| $u_k$ | Upper switches commutation/ modulation signals |
| $v_k$ | Lower switches commutation/ modulation signals |
| $x_5^d, x_5^q/v_c^d, v_c^q$ | Voltage on the capacitor C in the DQ frame |
| $x_6^d, x_6^q/i_L^d, i_L^q$ | Current to the grid in the DQ frame |
| $\mathbf{x}^{dq} = [x_5^d \; x_5^q \; x_6^d \; x_6^q]$ | Vectorial representation of the variables |
| $u/u^{dq}$ | Sum of the modulation signals/in the DQ frame |
| C/L | Capacitor/inductor of the second order filter |
| $w$ | Frequency of the grid |
| $\mathbf{J}$ | Jacobian of the map |

$$2v_{mpp} \leqslant g v_r^d \tag{14}$$
$$g = \frac{\sqrt{1-(Cwv_r^d/i_{pv})^2}}{1-LCw^2}$$

which reduces the conditions in such a way that $v_{pv}$ has a limit on the region that the panel can work, where the region is desired to contain to $v_{mpp}$, where $v_{mpp}$ is the PV voltage on the maximum power point.

## 4. Conditions for the compatibility of the converter

The previous approach only deals with operating points separately, even though the set has infinite elements of operating points. Thus there is the need to ensure that for every point in the $(i_{pv}, v_{pv})$ set there is a corresponding point on the set of output currents given by the $(x_6^d, x_6^q)$. This approach is based on the Inverse Function theorem [19,20] which states that if the set of points is continuous and the function which maps these elements to another set is continuous, then the image not only is continuous too but also there is a bijection from the preimage to the image set.

In order to use this theorem it is considered that the preimage set is the V-I surface with points $(i_{pv}, v_{pv})$ solution for the PV array, and the image set consist of the pair of currents $(x_6^d, x_6^q)$, which the converter delivers to the load/grid. If the equations which result from the converter interconnection accomplish the conditions stated by the theorem (being a continuous map), then for every point in the PV graph, the converter will be able to extract that power. It can be proved that the condition is fulfilled if the Jacobian of the map is non zero. Taking the equations of the converter and rearranging them it is obtained:

$$x_6^d = \frac{2v_{pv}i_{pv}}{v_r^d} \tag{15}$$
$$x_6^q = \frac{i_{pv}u^q + Cwv_r^d}{1-CLw^2} \tag{16}$$

which expresses the map from an $i_{pv}$ current to an $i_L$ current. Now obtaining the Jacobian as:

$$J = det\begin{pmatrix} \frac{\partial x_6^d}{\partial i_{pv}} & \frac{\partial x_6^d}{\partial v_{pv}} \\ \frac{\partial x_6^q}{\partial i_{pv}} & \frac{\partial x_6^q}{\partial v_{pv}} \end{pmatrix} = \frac{-2i_{pv}u^q}{v_r^d(1-CLw^2)}. \tag{17}$$

It can be noticed that the Jacobian of the map is non zero if the condition $u^q \neq 0, i_{pv} \neq 0$ is accomplished, then the converter successfully interconnects the PV array, where the voltage value of interest is $V_{mpp}$. An additional comment is that for the use of the converter is not strictly necessary for the map to be bijective (for the control it is). This property is very useful and easy to verify.

## 5. Simulation results

In this section simulation results of the system are presented under several scenarios in order to evaluate the compatibility. It is less complex and safer to make the test on simulations because one of the results to fail the conditions is the over modulation $|u| \geqslant 1$ with all the consequences that this implies. The simulation is done using the software Simulink from Matlab via the Sym Power Systems library for the two cells converter and a Solartech 1STH-215p model for the panel with $V_{mpp} = 26.3V$ and $I_{mpp} = 7.5$ for $Temp = 45°C$. In the simulations the peak value of the grid voltage is changed to $v_r^d = 143$ in order to test different scenarios, and the elements of the LC filter are $L = 10mH, C = 116\mu F$. The start sequence of the control and MPPT algorithm (incremental conductance) begin in $t = 0.4s$. Under this first scenario the compatibility condition in (14) is equal to:

$$v_{pv} \leqslant 53V \tag{18}$$

The above inequality means that the largest voltage on the PV array achievable before $|u| \geqslant 1$ is $v_{pv} = 53V$, if the $v_{mpp}$ is under this value but positive, then the system can achieve the MPP, and the condition is satisfied. Fig. 3 shows the current $i_{pv}$, the voltage $v_{pv}$ and the power $p_{pv}$ considering two panels in series connection where it can be seen the signals reach a stable operation point with an error in the $v_{mpp}$ close to $error_{vmpp} \leqslant 5v$. Fig. 4 shows the current $i_L$ which is sinusoidal once the steady state is reached.

Fig. 5 shows the modulation signal of one cell once the MPP is reached. It can be seen the modulation is close to 1 because the $v_{pv}$ is close to the limit $53V$. Fig. 6 shows the points where the PV array is working.

The second scenario corresponds to $v_{mpp} > 53V$, which is achieved connecting a three series array where the $v_{mpp} = 79V$. The Fig. 7 shows the current $i_{pv}$ the voltage $v_{pv}$ and the power $p_{pv}$, where it can be seen the signals reach an stable operation point close to the MPP. The stable working point is close to the MPP but does not satisfies (14) and this can be seen in the Figs. 8 and 9 where the $i_L$ current is highly distorted due to the modulation signal $u$ is in over modulation $u > 1$.

The Fig. 10 shows all the working point of the PV array.

The third case simulation considers a change in the radiation using steps from $1000W/m^2$ to $500W/m^2$ in $t = 10s$, and back to $1000W/m^2$ in $t = 20s$. The PV array in the simulations is a 2x2 array, with the same conditions as the previous cases.

Fig. 11 shows the current $i_{pv}$, the voltage $v_{pv}$ and the power $p_{pv}$, where it can be seen the signals reach an operating stable point close to the MPP in each radiation case. Figs. 12 and 13 show the output current $i_L$ once the stable working point in $1000W/m^2$ and $500W/m^2$ is reached, where the sinusoidal current can be seen.

## 6. Experimental results

A prototype of five-levels, two-cells ($n = 2$) MCR was built to evaluate the interconnection of a PV system (array of two panels in ERDM-250P6 in series connection) to a resistive load instead of the electrical grid. The switches used are integrated by and IGBT IRPF460 and a MUR860 diode. The parameters of the second order output filter are $L = 0.5$mH and $C = 10\mu$F with a resistive load $R_L = 39\Omega$. The cells have inductors $L_{hk/lk} = 120$mH with an associated winding resistance of $0.45\Omega$ each one. The DC bus is filtered by means of a capacitor $C = 1000\mu$F.

The system works in closed loop using the dSPACE DS1103 system where the control that interacts with the Maximum Power Point Tracking (MPPT) algorithm and the control for balancing the modules are programmed. An external resistance ($R_e = 0.45\Omega$) is connected in series with the cell inductor $L_{l2}$ in order to simulate a parametric variation and evaluate the performance of the control algorithm for the balance. The experimental setup configuration is shown in the Fig. 14.

The operating sequence of the prototype is as follows: First the system starts with the control and a variable resistance connected in parallel to the converter, to limit the rate of increase in the current of the converter. The variable resistance increases its value slowly to allow the rise of the current of the converter, to a certain point where the variable resistance value is similar to an open circuit impedance. Then, the current in the converter reaches the value $I_{pv}$, and the control for the balance of the modules is activated. Finally, when the error in the modules currents is close to zero, the MPPT and control for the current $i_L$ start.

The figures presented are recorded from the dSPACE system. The Fig. 15 presents the current $i_{pv}$, voltage $v_{pv}$ of the PV array and the instantaneous power $p_{pv} = v_{pv} * i_{pv}$ to obtain the instantaneous power delivered from the panel. In the interval 0 <t <325 s, the balancing algorithm is the only one in operation. Once the error due to unbalance is low enough, the MPPT algorithm is activated. From Fig. 15 it can be observed how the algorithm reaches a stable behavior that is reflected on the variables $v_{pv}, i_{pv}, p_{pv}$. The MPPT algorithm used is the classic perturb and observe; it is important to remark that the increments used in the MPPT algorithm are in the peak value of the current $i_L$. This is done because $i_L$ is used as the main signal to control for the power converter. The increment/decrement in $i_L$ is related to increment/decrement in $v_{pv}$ and $i_L$ used because the system is sub-actuated (not enough control signals to control both $v_{pv}$ and $i_L$). The relationship between increments/decrements in $v_{pv}$ and the peak value of $i_L$ can be observed form the Eqs. (10) and (12), where both signals are related via $u$. The selection of increments in the peak value $i_L$ is reflected in the form of the signals $v_{pv}$ and $p_{pv}$ (being quadratic).

Fig. 17 shows the current $i_L$ delivered to the resistive load $R_L$. It can be observed the sinusoidal form in the current (THD≈ 4%).

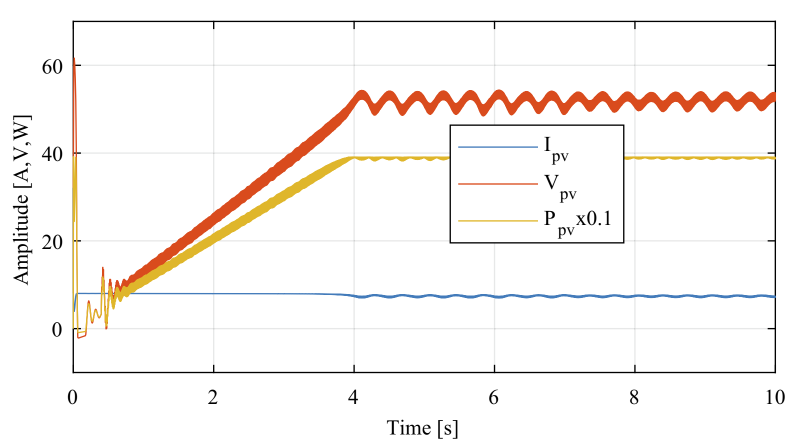


**Fig. 3.** Signals $v_{pv}, i_{pv}$ and $p_{pv}$ from the simulation with the compatibility conditions being satisfied.

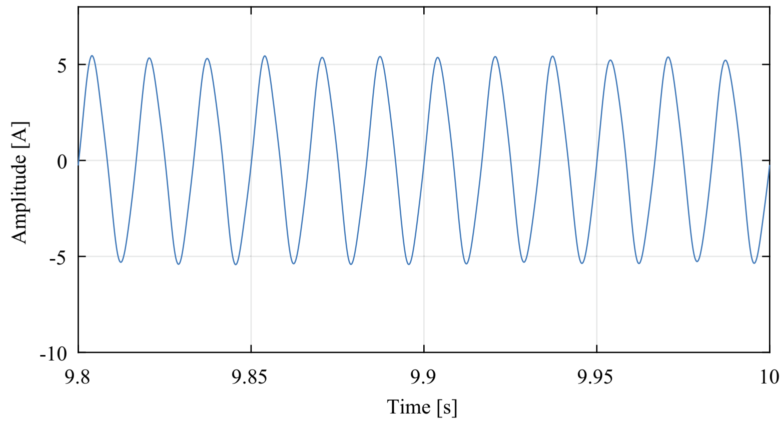


**Fig. 4.** Signal $i_L$ from the simulation with the compatibility conditions being satisfied.

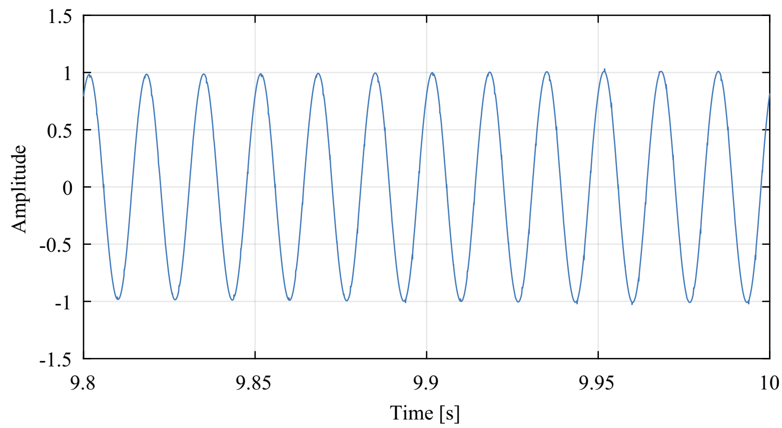


**Fig. 5.** Signal $u$ from the simulation with the compatibility conditions being satisfied.

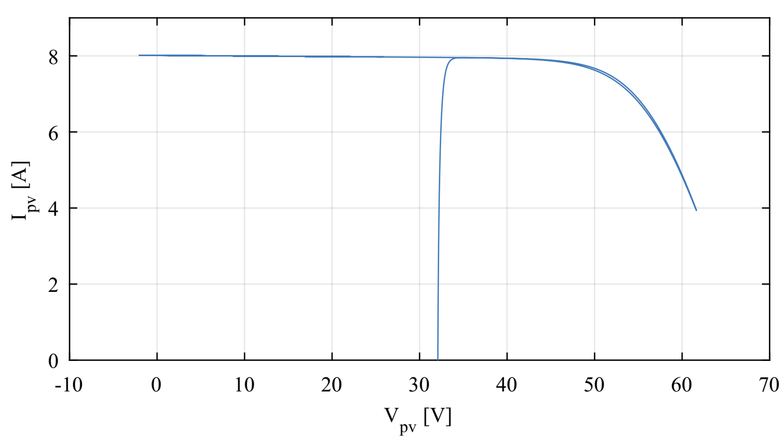


**Fig. 6.** $i_{pv} - v_{pv}$ graph where the compatibility is assured.

Fig. 18 shows the currents in the modules. It can be observed that they start with different values due to the unbalance condition imposed. After the control for the balance of the modules starts, their values tend to be the same ($i_{pv}/2$ in this case), all working together with the MPPT control. Also it can be observed the ripple in the currents due to the commutation and the voltage $v_c$. Fig. 19 presents the error in the current in the modules (being the reference $i_{pv}/2$), where it can be seen how the errors are close to zero (value 0.2A) which means the balance of the currents is achieved.

From the presented results it can be obtained:

- An error in the currents of the modules $< 0.2$ A (5%).
- A current $i_L$ with a THD of $\approx 4\%$.
- A power $\approx 440$ W form the PV array.
- An efficiency at the maximum power point of $\zeta \approx 0.88$

It is assumed that the point reached by the MPPT algorithm is the maximum of the PV array given the conditions at the time of the test and the power value reached by the MPPT algorithm.

It can be seen that for each operation point $(i_{pv}, v_{pv})$ in the panel in the Fig. 15, there is an output current $i_L$ as shown in the Fig. 16

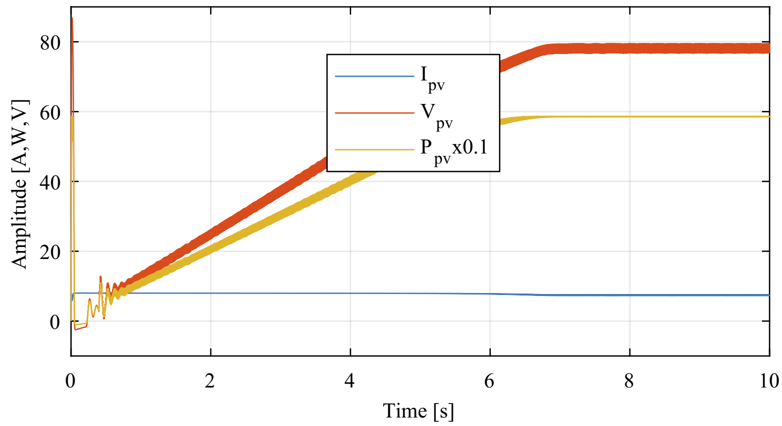


**Fig. 7.** Signals $v_{pv}, i_{pv}$ and $p_{pv}$ from the simulation with the compatibility conditions not being satisfied.

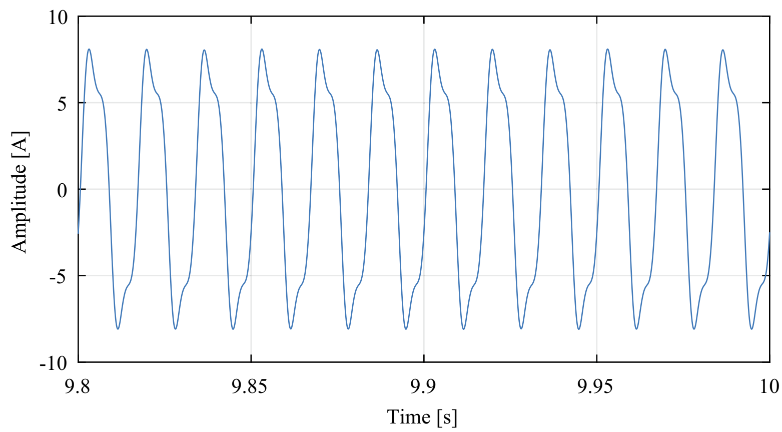


**Fig. 8.** Current $i_L$ form the simulation where the compatibility is not assured.

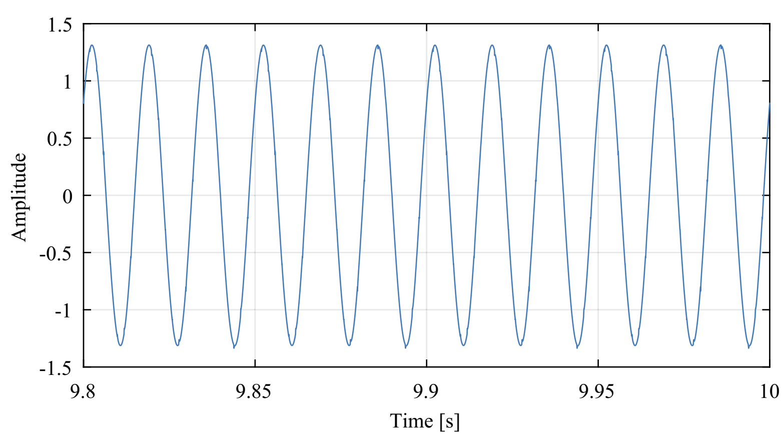


**Fig. 9.** Signal $u$ form the simulation where the compatibility is not assured.

(represented in the rms values of $i_L$ for easier view). Also, every point of power delivered form the panel $p_{pv}$ is mapped to an output power point $p_{out}$ as shown in the Fig. 20. Then the compatibility is proved at least in the region of interest (until the MPP), where the operations points used are shown in the Fig. 21. From this figure it can be seen part of the surface $(v_{pv}, i_{pv})$ under solar irradiations variations, which produces points "out" of the surface. These results are obtained with a resistive load instead of the AC mains, and represent the specific case where only active power is delivered to the load with control of $v_r^d$. Another difference is the condition (14) for the interconnection; now is $2v_{mpp} \leqslant gR_L i_L^d$, being this a more restrictive scenario because now the $i_L$ current and the $R_L$ load impose the maximum achievable voltage $v_{pv}$ on the panel.

## 7. Discussion of the results

The first simulation case evaluates the operation of the system at the edge of the working region. The second simulation scenario

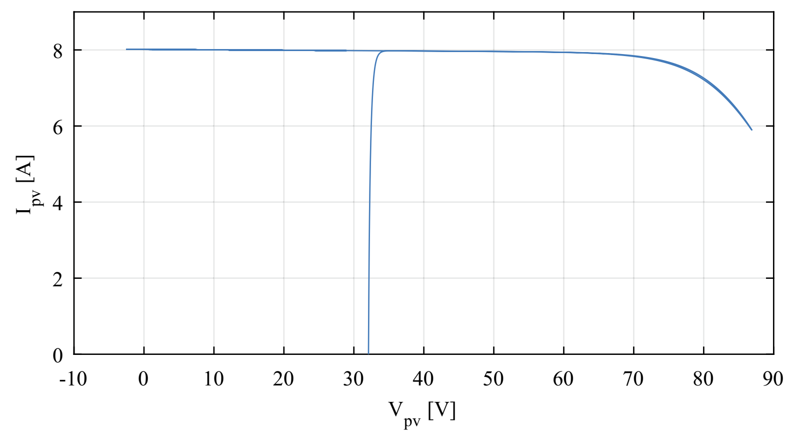


**Fig. 10.** $i_{pv} - v_{pv}$ graph form the simulation where the compatibility is not assured.

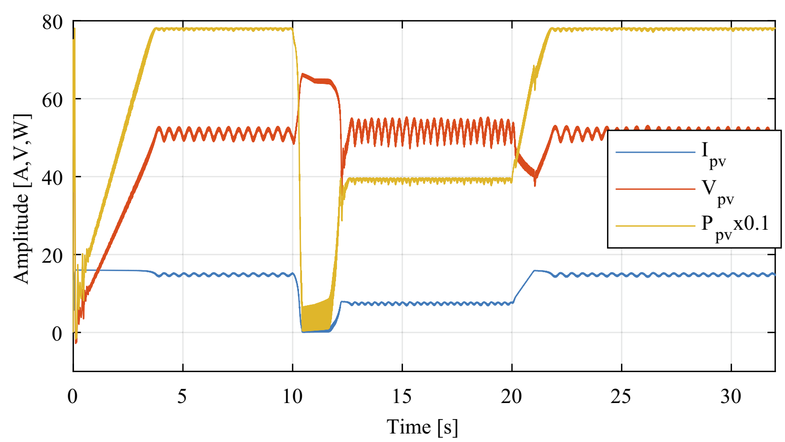


**Fig. 11.** Signals $v_{pv}, i_{pv}$ and $p_{pv}$ from the simulation under radiation changes.

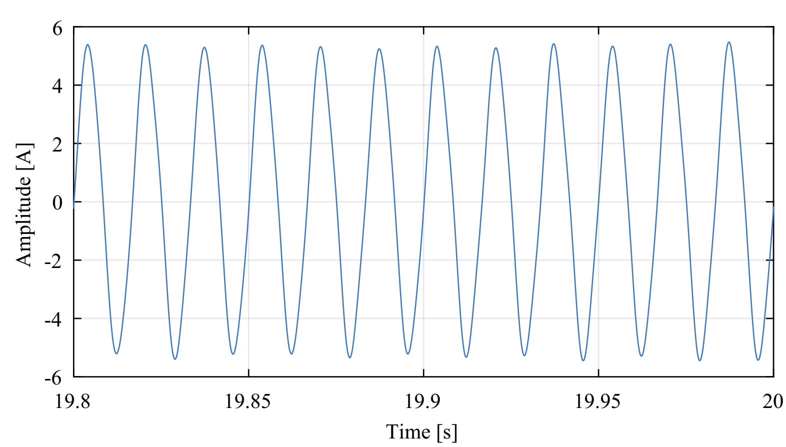


**Fig. 12.** Signal $i_L$ form the simulation under radiation changes.

verifies that it is not possible for the system to work outside the operating region, which is also experimentally verified. This illustrates the effectiveness of the method proposed in this work. From the scenario number one, accuracy of the procedure is obtained, where the system works in $V_{pv}$ close ≈0.5 V of the limit, and the magnitude of the modulation signal is ≈0.02 above the limit. The accuracy of the limit for the operating range is 1% of the measurement, which is calculated as error in $v_{pv}$/max value of $v_{pv}$. In scenario number two the current $i_L$ presents a THD of 23% when the magnitude of the modulation signal is 1.3 (operation in saturation) and the $v_{pv} = 79.1$V, which indicates that the system is not working correctly due to the high THD. Comparing the results of the present work with those of the literature there are similarities in the sense that there is an operation region that can be described from the converter model. The difference with previous works is that in them there is not a verification of the whole region but only an analytical verification of the region boundary. Another difference is that the related works only deals with DC-DC topologies, so

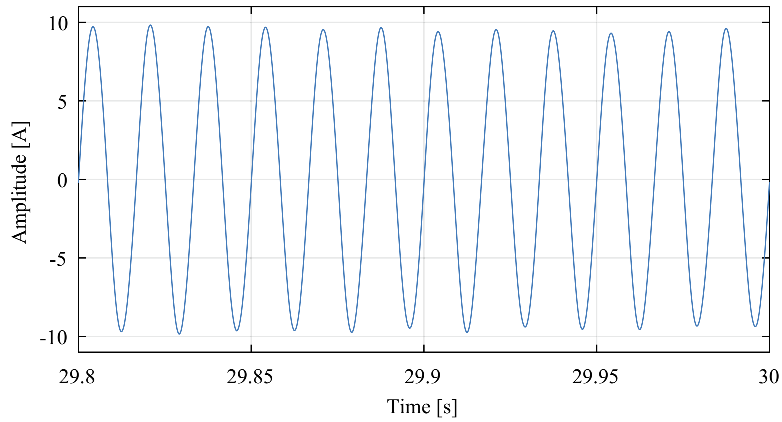


**Fig. 13.** $i_L$ from the simulation under radiation changes.

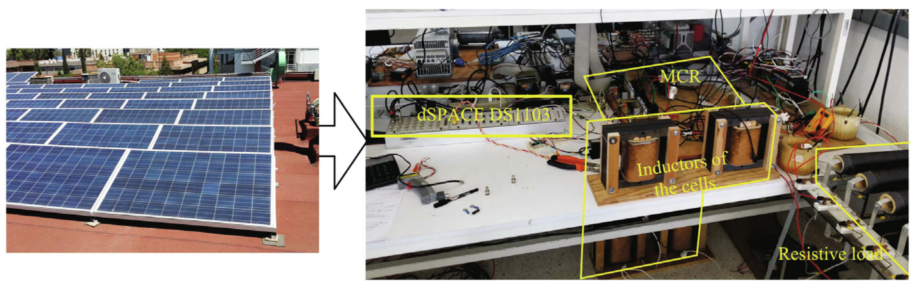


**Fig. 14.** Experimental prototype.

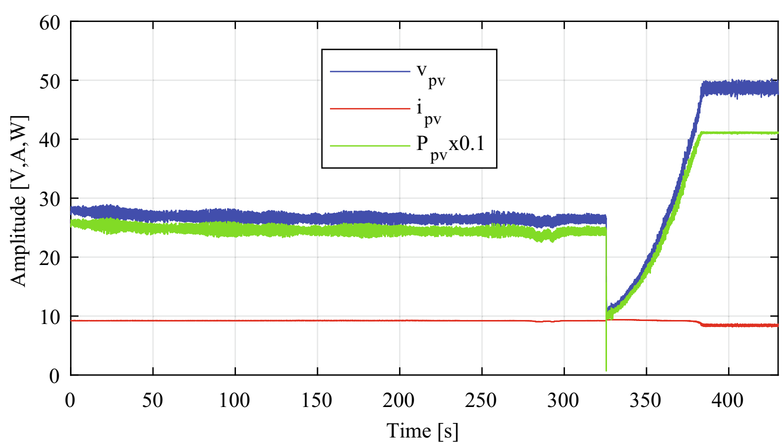


**Fig. 15.** Signals $i_{pv}$, $v_{pv}$ and $p_{pv}$ under unbalanced conditions.

the approaches are not fully comparable. The results support the use of more modular current source-based topologies for interconnection of renewable energy sources, and which can be studied in a similar way to the approach of this work. The only limitation to using the developed methodology is that the converter model in the DQ reference framework is required.

## 8. Conclusions

The experimental and simulation results verified the viability of the use of MCR as an interconnection element for the PV system and the load/grid. These results also proved the veracity of the conditions to reach the maximum power point and the operation in the region to reach the MPP and hence the compatibility. This proves the proposed model-based methodology to ensure the compatibility between the PV and MCR. It is important to mention that the model used is adequate for the compatibility study in the case of unbalanced conditions, due to the simplifications used. But the model is not necessarily suitable for the control of the converter if there are greater unbalanced conditions.

The study also includes the linkage of the MPPT algorithm with the control of the converter, which is essential because the common way to use the PV arrays is via a MPPT algorithm. The contribution of the work can be summarized in two principal points: first, to achieve the interconnection of a PV system via the MCR topology; second, to guarantee analytically and experimentally that the MCR-PV system works correctly. Both contributions are demonstrated by simulations and experimental results. The

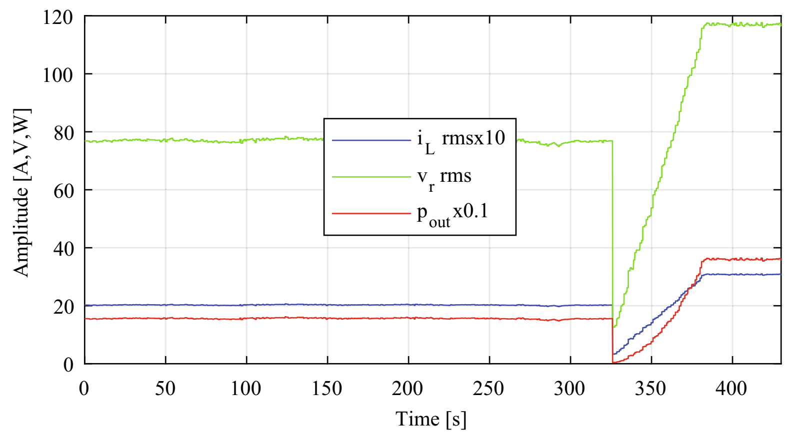


**Fig. 16.** Signals $i_L$ rms, $v_r$ rms and $p_{out}$ form the input and output of the MCR under unbalanced conditions.

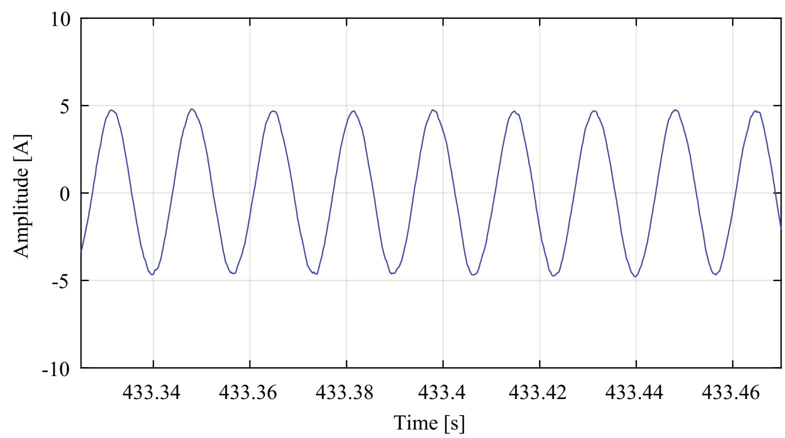


**Fig. 17.** Current $i_L$ delivered to the load $R_L$ under unbalanced conditions.

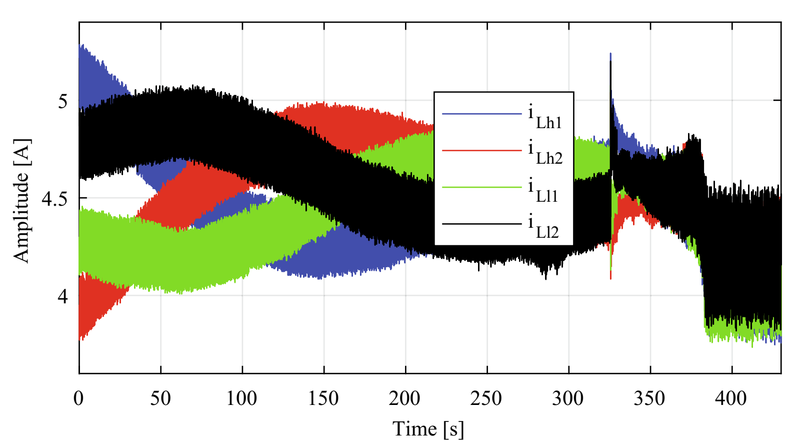


**Fig. 18.** Currents $i_{Lh1,2}, i_{Ll1,2}$ of the cells under unbalanced conditions.

operating range limits verified by simulations have an accuracy of 1% for proper operation with $THD_{iL}$ = 4% inside the operating range and $THD_{iL}$ = 23% outside the range. Also remembering the precision $< 5$V of the MPPT algorithm together with the MCR to reach the MPP. The scientific value of the work is in verifying adding the option of the MCR as an interconnection topology for renewable sources, where the converter has properties that can benefit to the PV systems. The methodology and tools used in this research work to test the operation of the system can help to complement the lack of formal tools to select viable topologies for interconnecting photovoltaic systems. The applicability of the results is directly in the design and use of the MCR in PV applications because the research is focused on that topology but the methodology is based on the converter model and its equilibrium points it can be used in other topologies. The limitation of the approach lies in the fact that it is only valid for the steady state operation of the system, so in

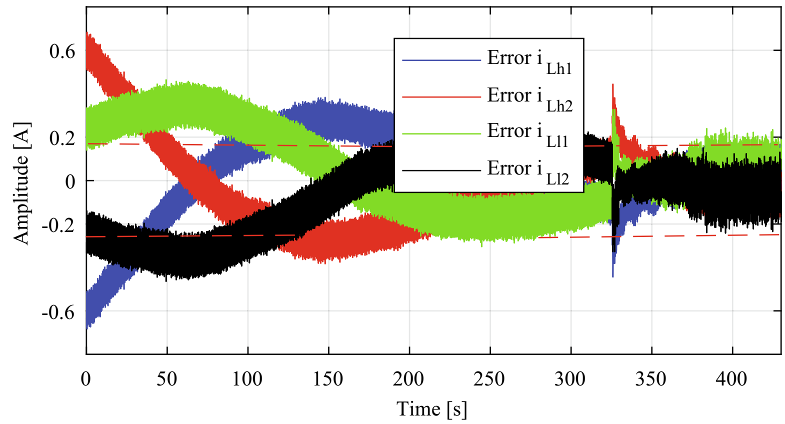


**Fig. 19.** Errors in the currents $i_{Lh1/2}, i_{Ll1/2}$ under unbalanced conditions.

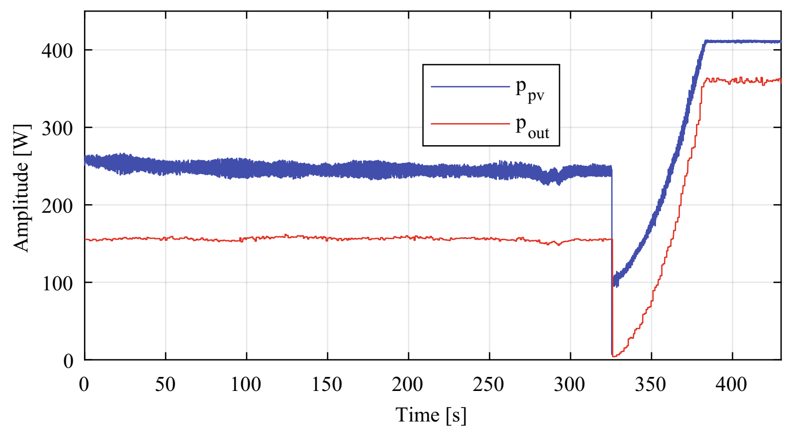


**Fig. 20.** Power $p_{pv}$ from the panel and output power $p_{out}$ under unbalanced conditions.

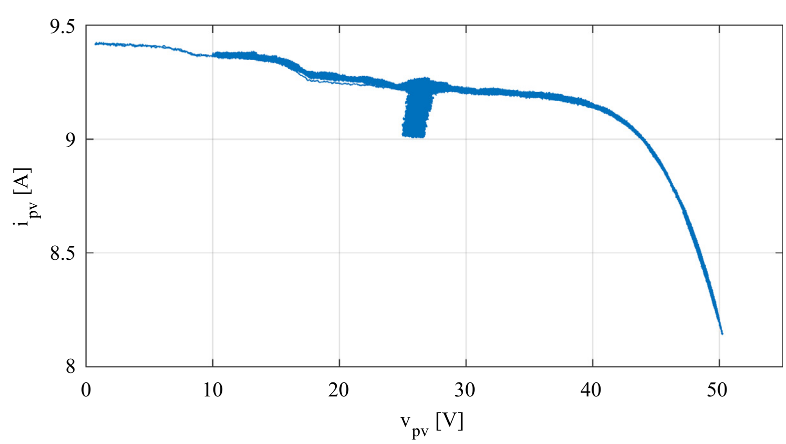


**Fig. 21.** $v_{pv}$ versus $i_{pv}$ from the panel.

transients is not assured that the system works correctly. Another limitation is that the condition is not restrictive, which means that if the condition is not achieved it does not mean that the system is incompatible. In this sense, possible future work will be aimed in ensuring compatibility even in transients, and to establish a more restrictive condition for the compatibility. A final point to highlight is the need of tools to facilitate the selection of topologies and the corroboration of the topologies used to interconnect PV systems with the electrical grid/loads in the design phase; before the construction and operation of the system so that errors and problems can be reduced or avoided.

## Declaration of Competing Interest

The authors declare that they have no known competing financial interests or personal relationships that could have appeared to influence the work reported in this paper.

## Acknowledgements

This research work was supported by the project UASLP - LiCORE AC, AG- 271/18. The authors would like to thank the National Council of Science and Technology of Mexico (CONACyT) for the academic scholarship under the Grant No. 554924, and the UNAM under the grant DGAPA-PAPIIT IN118019.

## References

[1] Kibaara SK, Murage DK, Musau P, Saulo MJ. Comparative analysis of implementation of solar PV systems using the advanced SPECA modelling tool and HOMER software: Kenyan scenario. HighTech Innov J 2020;1(1):8–20. doi: https://doi.org/10.28991/HIJ-2020-01-01-02.

[2] Borowski PF. New technologies and innovative solutions in the development strategies of energy enterprises. HighTech Innov J 2020;1(2):39–58. doi: https://doi.org/10.28991/HIJ-2020-01-02-01.

[3] Uzum B, Onen A, Hasanien HM, Muyeen SM. Rooftop Solar PV Penetration Impacts on Distribution Network and Further Growth Factors A Comprehensive Review. Electronics 2021;10(1):55. doi: https://doi.org/10.3390/electronics10010055.

[4] Okawa T, Honbu M, Matsuda Y, Shibata T, Kawaguchi T. Twelve-step current source inverter; June 30 1981. US Patent 4,276,589.

[5] Ahmed BM, ALhialy NFF. Optimum efficiency of PV panel using genetic algorithms to touch proximate zero energy house (NZEH). Civil Eng J 2019;5(8):1832–40. doi: https://doi.org/10.28991/cej-2019-03091375.

[6] Selem SI, ElFergany AA, Hasanien HM. Artificial electric field algorithm to extract nine parameters of triplediode photovoltaic model. Int J Energy Res 2021;45(1):590–604. doi: https://doi.org/10.1002/er.5756.

[7] Qais MH, Hasanien HM, Alghuwainem S. Transient search optimization for electrical parameters estimation of photovoltaic module based on datasheet values. Energy Convers Manage 2020;214:112904. doi: https://doi.org/10.1016/j.enconman.2020.112904.

[8] Moosavain SM, Hizam Hashim, Hamiruce Marhaban M, Taghvaee MH, Radzi MAM. A current and future study on non-isolated dc-dc converters for photovoltaic applications. Renew Sustain Energy Rev 2013;17:216–27. https://doi.org/10.1016/j.rser.2012.09.023.

[9] Duran E, Sidrach-de-Cardona M, Galan J, Andujar JM. Comparative analysis of buck-boost converters used to obtain i–v characteristic curves of photovoltaic modules. In: 2008 IEEE Power Electronics Specialists Conference. p. 2036–42. doi: https://doi.org/10.1109/PESC.2008.4592243.

[10] Suresh Amarnath Kurella R. Simulation of incremental conductance MPPT with direct control method using Cuk converter. Int J Res Eng Technol 2013;02(09):557–66. doi: https://doi.org/10.15623/ijret.2013.0209086.

[11] Wang HX, Muñoz-García MA, Moreda GP, Alonso-García MC. Optimum inverter sizing of grid-connected photovoltaic systems based on energetic and economic considerations. Renew Energy 2018;118:709–17. doi: https://doi.org/10.1016/j.renene.2017.11.063.

[12] Singh SN. Selection of non-isolated DC-DC converters for solar photovoltaic system. Renew Sustain Energy Rev 2017;76:1230–47. doi: https://doi.org/10.1016/j.rser.2017.03.130.

[13] Ramki T, Tripathy LN. Comparison of different DC-DC converter for MPPT application of photovoltaic system. In: International Conference on Electrical, Electronics, Signals, Communication and Optimization (EESCO); 2015, January. p. 1–6. doi: 10.1109/eesco.2015.7253764.

[14] Litrán SP, Durán E, Semião J, Barroso RS. Single-Switch Bipolar Output DC-DC Converter for Photovoltaic Application. Electronics 2020;9(7):1171. doi: https://doi.org/10.3390/electronics9071171.

[15] Kumar GR, Bandaru RK. Single phase PV-fed current source inverter with sinusoidal grid current injection control. In: 2019 International Conference on Electrical, Electronics and Computer Engineering (UPCON); 2019. p. 1–5. https://doi.org/10.1109/upcon47278.2019.8980138.

[16] Reddy VU, Reddy KM, BABU GVS. Performance analysis of hybrid power system with current source grid inverter. Int J Adv Technol Innov Res 2015;07(20):3947–52.

[17] Guzman JI, Perez MA, Melin PE, Espinoza JR, Baier CR. Predictive control of modular current source converters. In: IECON 2014–40th Annual Conference of the IEEE Industrial Electronics Society; 2014. p. 1720–1726. DOI: 10.1109/IECON.2014.7048734.

[18] Bai Z, Ma H, Xu D, Wu B. Control strategy with a generalized dc current balancing method for multimodule current-source converter. IEEE Trans Power Electron 2014;29(1):366–73. doi: https://doi.org/10.1109/TPEL.2013.2252628.

[19] Wendell Fleming. Functions of several variables. Springer; 2012. https://doi.org/10.1007/978-1-4684-9461-7.

[20] Apostol Tom. Mathematical Analysis. Addison-Wesley; 1981 5th edition. https://doi.org/10.1515/9781400839551-006.

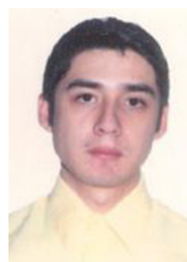

**Rafael de Jesús Hernández Hernández** received the B.Sc. in mechatronic engineering from Technological Institute of San Luis Potosí in 2012, and M.Sc. in electrical engineering from Autonomous University of San Luis Potosi in 2016. He is currently working toward the Ph.D. degree in electrical engineering at the Autonomous University of San Luis Potosi, México. His research interests are focused in the study of current source converters, especially aimed at the modeling, controlling and sizing, modular/multilevel current source converter and the interconnections of renewable energy sources.